Princeton Plasma Physics Laboratory

PPPL- 4747

PPPL- 4747

Free MHD Shear Layers In The Presence Of Rotation And Magnetic Field

E.J. Spence, A.H. Roach, E.M. Edlund, P. Sloboda and H. Ji

March, 2012

PPPL PRINCETON PLASMA PHYSICS LABORATORY

Prepared for the U.S. Department of Energy under Contract DE-AC02-09CH11466.

Princeton Plasma Physics Laboratory
Report Disclaimers

Full Legal Disclaimer

Trademark Disclaimer

PPPL Report Availability

Princeton Plasma Physics Laboratory:

http://www.pppl.gov/techreports.cfm

Office of Scientific and Technical Information (OSTI):

http://www.osti.gov/bridge

Related Links:

U.S. Department of Energy

Office of Scientific and Technical Information

Fusion Links

Free MHD shear layers in the presence of rotation and magnetic field

E. J. Spence[1, a)] and A. H. Roach, E. M. Edlund, P. Sloboda and H. Ji[1]

Center for Magnetic Self-Organization in Laboratory and Astrophysical Plasmas and Princeton Plasma Physics Laboratory, Princeton, NJ 08543, USA

(Dated: 14 March 2012)

We present an experimental and numerical study of hydrodynamic and magnetohydrodynamic free shear layers and their stability. We first examine the experimental measurement of globally unstable hydrodynamic shear layers in the presence of rotation, and their range of instability. These are compared to numerical simulations, which are used to explain the modification of the shear layer and thus the critical Rossby number for stability. Magnetic fields are then applied to these scenarios, and globally unstable magnetohydrodynamic shear layers generated. These too are compared to numerical simulations, showing behavior consistent with the hydrodynamic case and previously reported measurements.

[a)]Electronic mail: ejspence@pppl.gov

I. INTRODUCTION

A shear layer is a layer of flowing fluid which possesses a velocity field gradient in a direction orthogonal to the flow. Such layers are common in fluid flow near boundaries, where the fluid must typically reach zero velocity at the bounding wall. A shear layer is called 'free' when it exists in the absence of a boundary. Such layers generally exist when discontinuities in the boundary conditions of a flow are subject to some manner of stabilizing force, such as the Coriolis or Lorentz force. This stabilization allows the discontinuity to penetrate into the bulk of the fluid as a shear layer. Such layers may exist naturally in geophysical[1,2] or stellar systems[3,4].

Hydrodynamic free shear layers were first discussed theoretically by Proudman[5] and Stewartson[6], who examined systems of fluid under rapid rotation subject to a boundary discontinuity that was only slightly differentially rotating, allowing the discontinuity in the flow to be treated linearly. The prediction of the thickness of such shear layers, which became known as Stewartson layers, and their scaling with Ekman number, $E = \nu/(a^2\Omega_2)$, where ν is the fluid's kinematic viscosity, a is a length scale and Ω_2 is the global rotation rate, was a triumph of the theoretical analysis of such flows. These predictions were later confirmed both experimentally[7,8] and numerically[9,10].

Not surprisingly, if there is enough free energy in the shear layer the layer will become unstable to a Kelvin-Helmholtz-type instability, sometimes called a barotropic instability. This has been observed by a number of experimental groups in cylindrical hydrodynamic studies[7,11–14]. The instability manifests itself as a set of two-dimensional eddies which roll up in the $r-\theta$ plane, where we are using the standard cylindrical coordinates (r, θ, z). The azimuthal mode number of the instability depends on a number of factors, especially the differential speed across the boundary discontinuity which generates the shear layer and the amount of global rotation. These are parameterized by the Rossby number, $Ro = \Delta\Omega/\Omega_2$, where $\Delta\Omega = \Omega_1 - \Omega_2$ is the angular speed difference across the boundary discontinuity, and the Ekman number E, defined above. When both Ro and E are small enough the shear layer tends to be stable, but when the Rossby number gets too large the layer destabilizes, with the scaling of the critical Rossby number depending upon the geometry of the system[15], a result also observed in numerical simulations of spherical Couette flow[16–19].

In contrast to the much-larger corpus of work on hydrodynamic free shear layers, relatively

little work has been done studying their magnetohydrodynamic (MHD) analogy: free shear layers which are generated by the Lorentz force instead of the Coriolis force. Just as the Coriolis force causes rotating flows to become independent of the ordinate along the axis of rotation, so too can magnetic fields cause flows of electrically conducting fluid to become independent of the ordinate parallel to the direction of the applied field. Such free shear layers, now known as Shercliff layers[19], have been studied both experimentally[20–22], and numerically[19,23–25]. Like their hydrodynamic cousins, these shear layers are unstable to a Kelvin-Helmholtz-type instability when the amount of shear becomes large relative to the restoring force.

Unlike the hydrodynamic case, where there have been theoretical analyses of small differential rotation of the boundary discontinuity[6], there have been no analytical studies examining the role of magnetic field in shear-layer stabilization in the absence of global rotation. This is due to the fact that without only a small amount of differential rotation the Navier-Stokes equation remains strongly nonlinear despite the magnetic field, and thus analytically intractable. We must, consequently, turn to numerical simulations to make progress on this topic.

In this paper we extend a previous study of free MHD shear layers by Roach and collaborators[22] to examine the effect of global rotation on the stability of such layers in the regime of large Rossby number, $Ro \sim \mathcal{O}(1)$. We also examine the suppression of these shear layers by secondary circulation. Two tools are used in this study: the Princeton MRI experiment and 2D numerical simulations; these are presented in Section II. In section III we show how the large-Rossby number limit eventually results in the absence of a globally-unstable hydrodynamic shear layer. Numerical simulations are used to elucidate these results. These now-locally-unstable shear layers can be made globally unstable using a magnetic field; measurements demonstrating this are presented in Section IV. We conclude with a discussion of these results and avenues for further study.

II. TOOLS FOR STUDYING SHEAR LAYERS AND THEIR STABILITY

In this work we use two tools to examine the roles of global rotation and magnetic field on the generation of free shear layers and their stability. These are the Princeton magnetorotational instability (MRI) experiment, and 2D numerical simulations of the experiment

TABLE I. Experimental parameters of the Princeton MRI experiment.

Height	h	0.279 m
Inner-cylinder radius	r_1	0.071 m
Outer-cylinder radius	r_2	0.203 m
Ring-junction radius	r_0	0.137 m
Radial gap	a	0.132 m
Density	ρ	6360 kg/m^3
Kinematic viscosity	ν	3.0×10^{-7} m^2/s
Magnetic diffusivity	η	0.257 m^2/s
Axial magnetic field	B	0 - 0.45 T

performed using the ZEUS-MP code.

A. Princeton MRI experiment

The Princeton MRI experiment is a Taylor-Couette apparatus which uses the gallium eutectic GaInSn as its working fluid[26]. A schematic of the experiment is presented in Figure 1. To suppress the secondary circulation which develops due to the Ekman layers at the top and bottom of the experiment, the endcaps which vertically contain the fluid are split into two independently rotating rings, giving the experiment four rotation rates: those of the inner cylinder, inner ring, outer ring and outer cylinder. The differential rotation at the inner ring-outer ring junction breaks up the secondary circulation, resulting in less-turbulent flow. Axial magnetic fields are applied to the experiment by a set of six external magnetic field coils, giving an applied field of up to 0.45 Tesla. Parameters for the experiment are given in Table I.

The velocity field of the experiment is measured using an ultrasonic Doppler velocimetry (UDV) system[27]. Ultrasonic transducers are mounted to the outer cylinder at the midplane of the experiment and just above the lower endcap rings. The transducers are oriented tangential to the inner cylinder, allowing the azimuthal velocity to be measured. Transducers are placed at two azimuthal locations at the midplane, allowing information about the azimuthal mode structure of the destabilized free shear layers to be gathered. Signals from

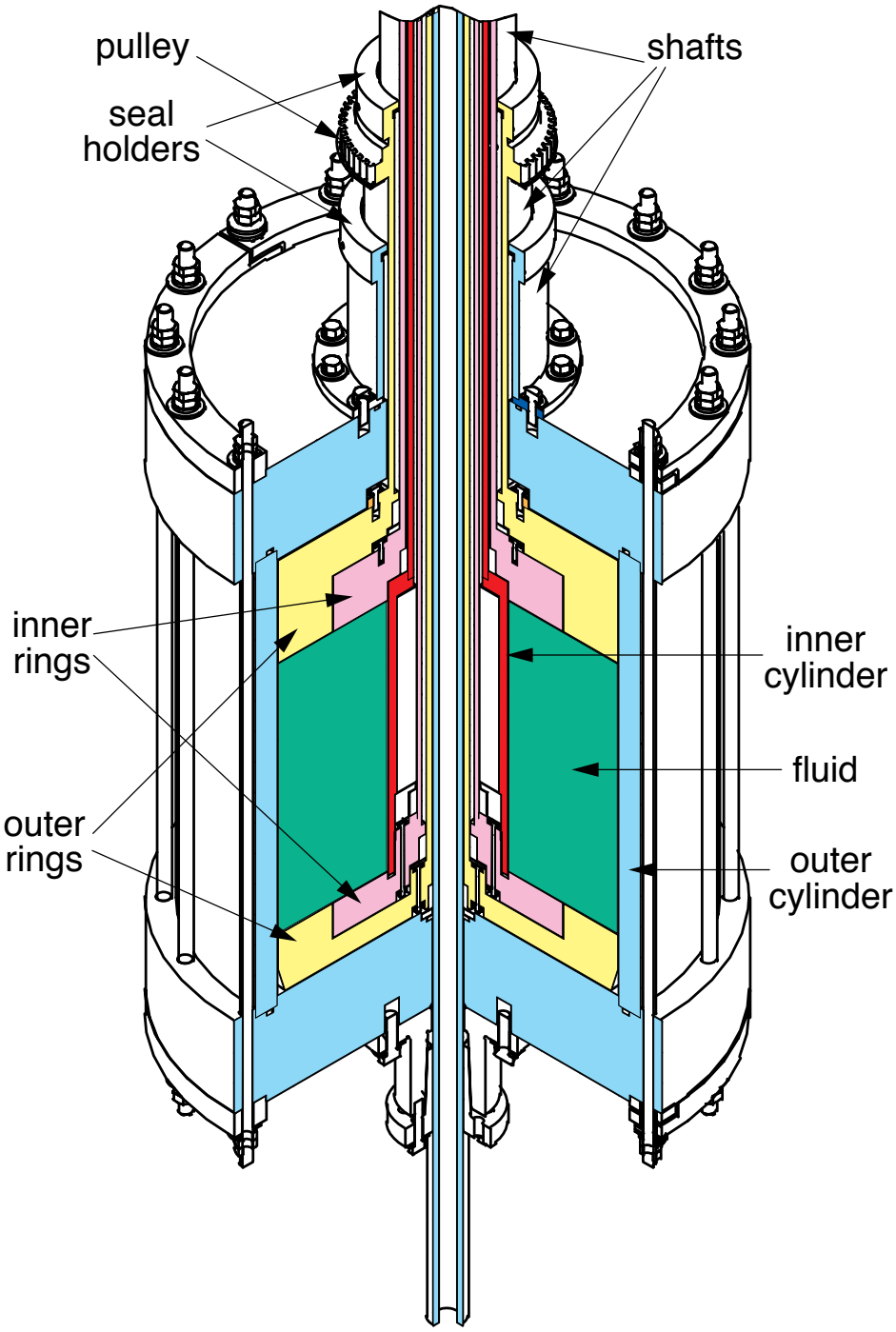

FIG. 1. Schematic of the Princeton MRI experiment. Note the differentially rotatable top and bottom endcap rings, which can generate a discontinuity in the azimuthal-flow boundary condition.

the transducers are passed through a slip-ring to move the signal to the laboratory frame.

For the experiments used in this study, the inner-cylinder and inner-ring rotation rates were identical, and the outer-ring and outer-cylinder rotation rates were also matched. This resulted in only two rotation rates for these experiments, with the discontinuity in rotation rate occurring at the inner ring-outer ring junction. This velocity field discontinuity generated the shear layers which are the subject of this study. These rotation rates are listed with the notation (Ω_1, Ω_2) in this paper, corresponding to (inner speed, outer speed) in revolutions per minute.

B. 2D simulations

Numerical simulations can be a useful tool for exploring experimentally inaccessible regimes, as well as determining the dynamics of areas of the experiment which are difficult to diagnose. For this study we use the ZEUS-MP 2.0 code[28], to which viscosity and resistivity have been added[29]. The code solves the Navier-Stokes and magnetic induction equations in multiple geometries, in this case cylindrical. The code is time-explicit, compressible and three-dimensional, though axisymmetry is enforced for this study, and an incompressible limit is taken. The boundary conditions on the flow are no-slip on the various rotating surfaces. The magnetic field at the boundaries is matched to the external vacuum solution[30]. Applied magnetic fields are generated using external current distributions which closely resemble those of the experiment. Further details of the implementation of the code to simulate this experiment have been given previously[31].

All simulations used in this study were performed with a resolution of 256 radial and 512 vertical points. A kinematic viscosity 300 times that of the experimental working fluid was used, as well as an electrical conductivity 3 times too high, resulting in a magnetic Prandtl number of $Pm = \nu/\eta = 10^{-3}$. The list of simulations used in this paper, with their associated dimensionless parameters, is given in Table II.

III. SUPPRESSION OF THE HYDRODYNAMIC SHEAR LAYER

As discussed above, hydrodynamic free shear layers can form in rotating systems in the presence of a discontinuity in the velocity field boundary condition. The Princeton MRI

TABLE II. Parameters of the simulations used in this work.

Ω_1 [rev/min]	Ω_2 [rev/min]	B [G]	E	Ro	Λ
350	100	0.0	5.6×10^{-4}	2.5	0.0
400	100	0.0	5.6×10^{-4}	3.0	0.0
400	100	800.0	5.6×10^{-4}	3.0	0.25
400	100	1600.0	5.6×10^{-4}	3.0	1.0
400	100	3580.0	5.6×10^{-4}	3.0	5.0
400	100	5060.0	5.6×10^{-4}	3.0	10.0
175	50	0.0	1.1×10^{-3}	2.5	0.0
200	50	0.0	1.1×10^{-3}	3.0	0.0
1750	500	0.0	1.1×10^{-4}	2.5	0.0
2000	500	0.0	1.1×10^{-4}	3.0	0.0

experiment, with its independently-rotating endcap rings, has such a boundary discontinuity, and consequently we expect such shear layers to form. Since it has been demonstrated experimentally[7,11–14,32], numerically[16–19,25], and analytically[15,33] that such free shear layers destabilize when the amount of shear becomes sufficient, we also expect the shear layers in the experiment to be unstable. The transition of the hydrodynamic shear layer to instability has been found[15] to occur at a critical Rossby number of $Ro_{\rm crit} \sim E^{3/4}$ in a cylindrical geometry. This relationship has been roughly confirmed by experiment[7,14,32]. For the Princeton MRI experiment $Ro_{\rm crit} \sim 10^{-5}$; unfortunately such a small amount of differential rotation is beyond the technical capabilities of this apparatus, and thus the stable regime, where $Ro < Ro_{\rm crit}$, has never been observed.

Nonetheless, experimental evidence for a destabilized hydrodynamic shear layer in the Princeton MRI experiment has been observed. This is presented in Figure 2, which shows the azimuthal flow at a radial location as a function of time, for the speeds (270, 100). The two timeseries are from two UDV transducers which are offset azimuthally by 90°, indicating that the instability likely has saturated as an $m = 1$ mode, where m is the azimuthal mode number, since the two timeseries are 90° out of phase. This is consistent with previous reports, which show that higher-Rossby number regimes, such as in this study, result in lower azimuthal mode numbers in the instability's saturated state[7,14]. The spatial structure

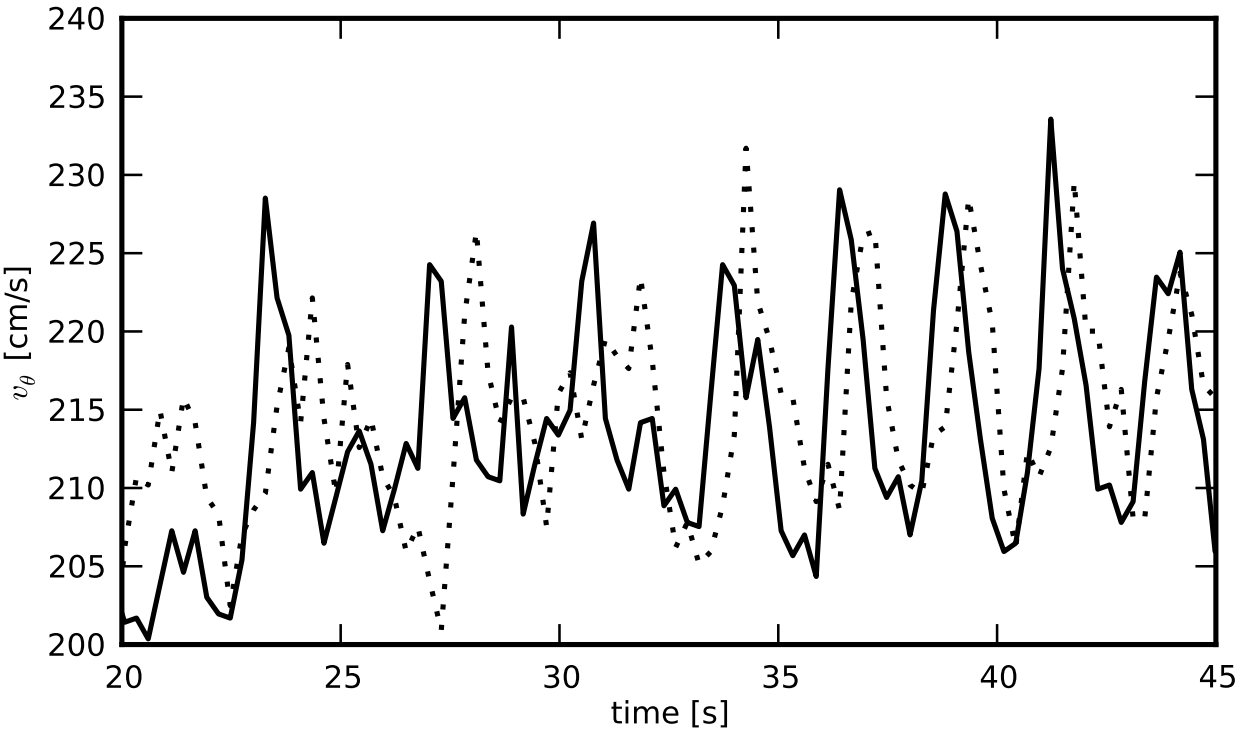

FIG. 2. Azimuthal velocity at $r = 18.2$ cm versus time, measured at the midplane at $\theta = 0$ (solid) and at $z = 3$ cm at $\theta = \pi/4$ (dotted), for (270, 100), no applied field.

of the mode, as swept out by a chord of UDV measurements over one oscillation period, is presented in Figure 3. The spiral structure previously observed in this apparatus, due to a magnetic field-induced free-shear-layer instability, is reproduced[22], strongly suggesting that this is the purely-hydrodynamic version of the free-shear-layer instability. Consistent with other results[22], the instability is observed to be global, filling the volume of the apparatus, vertically independent (as far as can be measured), and rotates at a frequency of about 30% of the average of the rotation speeds, $f_{\rm rot} \sim 0.3(\Delta\Omega/2)$, in the rotating frame. The destabilized mode is a robust feature of the experiment, consistently observed over a range of Ekman numbers.

There is a limit to the range of Rossby numbers over which the hydrodynamic free-shear-layer instability is observed. In Figure 4 we present an example of a measured azimuthal velocity timeseries which is just above the critical Rossby number for stabilization of the instability. As can be seen, the instability is driven during the spin-up phase of the experiment, but as the mean flow becomes established the instability is eventually damped away. The measured value of Ω_1 which stabilizes the global shear-layer instability, for a given

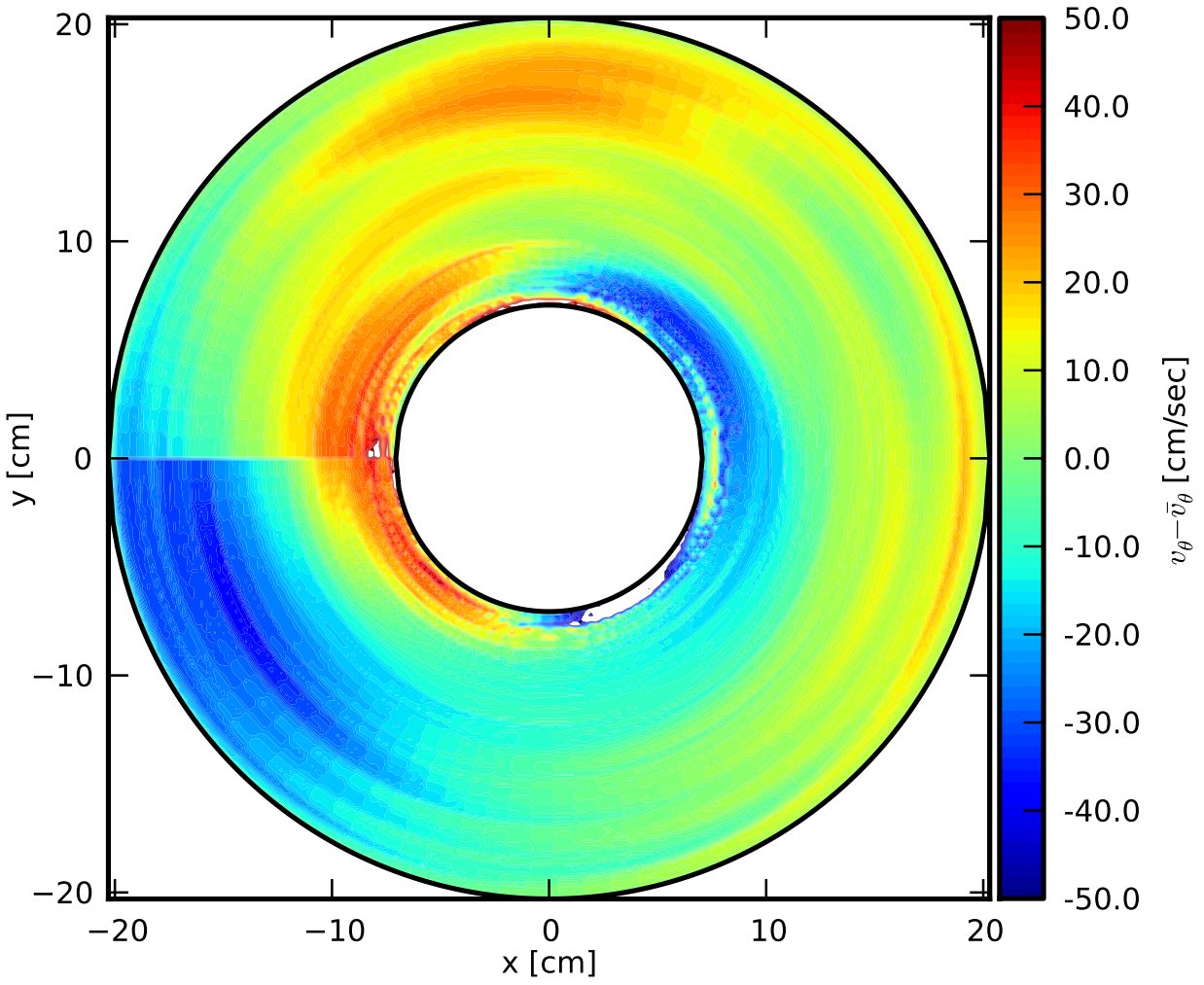

FIG. 3. Spatial structure of the measured azimuthal flow over one period of oscillation, at the midplane, with the axisymmetric background removed, for (270, 100), no applied field.

value of Ω_2, is presented in Figure 5. The curve corresponds to a value of $Ro = 2.35$, which interestingly is a constant for the range of rotation rates examined, though admittedly this corresponds to a small range of Ekman number, $3.7 \times 10^{-6} \leq E \leq 6.1 \times 10^{-7}$.

No theoretical or experimental discussion has been given to the topic of the suppression of the hydrodynamic free-shear-layer instability by increasing Ro far above $Ro_{\rm crit} \sim E^{3/4}$. This is not surprising, given that once $Ro \sim \mathcal{O}(1)$ the assumption that the nonlinearities of the system are unimportant is no longer valid, making analytic treatment of the problem difficult. To address this issue we turn to numerical simulations, an example of which is presented in Figure 6. This displays a snapshot of the contours of both the poloidal stream function and the shear, which we define here as $q = (r/\Omega)\,\partial\Omega/\partial r$, where $\Omega = v_\theta/r$ and v_θ

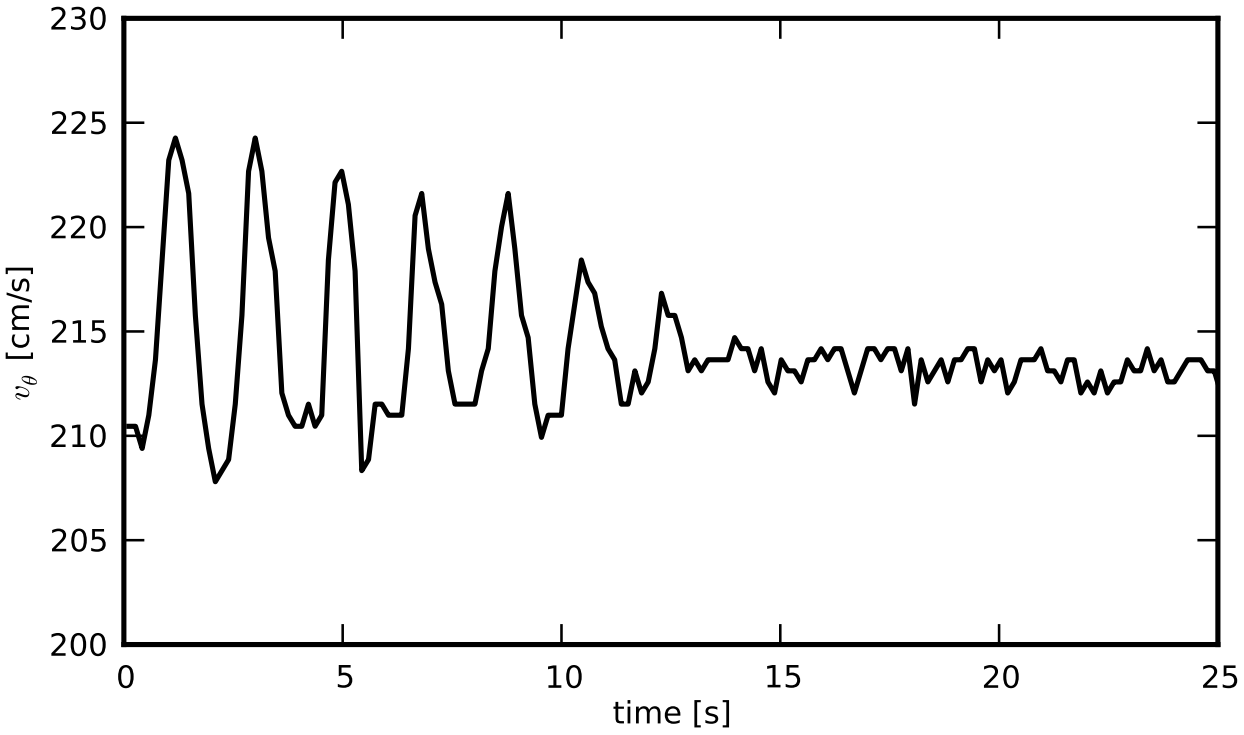

FIG. 4. Azimuthal velocity at $r = 18.2$ cm versus time, measured at the midplane, for (335, 100), no applied field.

is the azimuthal flow, for the case of (350, 100) with no applied field, which corresponds to $Ro = 2.5$. As can be seen, a clear hydrodynamic free shear layer is formed just outside the inner ring-outer ring junction, and penetrates into the bulk of the fluid. Poloidal circulation cells form on either side of the shear layer. As the Rossby number is increased the shear layer no longer extends vertically into the center of the fluid, but rather is pushed outward radially by the secondary circulation. This is shown in Figure 7, which presents the case of (400, 100) with no applied field, $Ro = 3.0$.

As the shear layer in the simulations penetrates into the bulk of the fluid we would expect that, if these were 3D simulations, the layer would become globally Kelvin-Helmholtz unstable, generating the oscillating signals in the azimuthal flow which are measured in the experiment. One can hypothesize that, as the Rossby number is increased and the shear layer is pushed radially outward, the shear layer would not become globally unstable such that the bulk of the fluid is also destabilized, but rather would be merely locally unstable, generating turbulence near the endcaps. This explains the lack of large-scale oscillations in the experiment for $Ro \geq 2.35$, and as such the behavior of the shear layers in the simulations

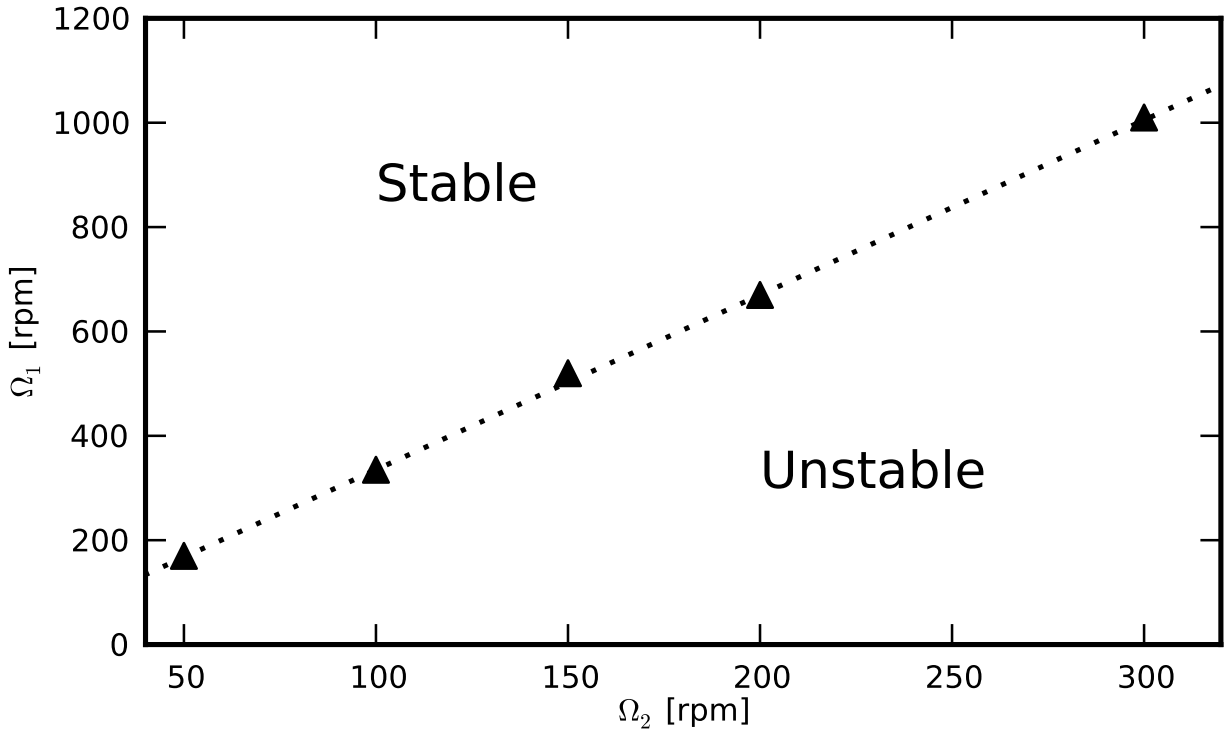

FIG. 5. Value of Ω_1 which suppresses the global free-shear-layer instability versus Ω_2. The linear trend corresponds to $Ro = 2.35$.

as the Rossby number is increased is consistent with experimental measurements. The question remains of how the shear layers which do not penetrate all the way to the midplane of the experiment generate a vertically independent mode throughout the bulk of the fluid. We will revisit this question in Section V.

IV. MAGNETIZED SHEAR LAYER DESTABILIZATION

If we now restrict our experimental studies to the regime where $Ro = 2.35$, thus ensuring that the system has a hydrodynamic shear layer which is not globally unstable, we can examine the role that an applied magnetic field plays in generating a magnetized free shear layer. A representative timeseries of such a case is displayed in Figure 8, which presents the azimuthal flow versus time for speeds of (670, 200) and an applied field of 3440 G. Initially, before the field is applied, there is no evidence of shear layer instability. However, when the field is applied the instability grows and saturates, much like the measurements reported by Roach *et al.*[22]. When the field is removed the flow returns to its initial state.

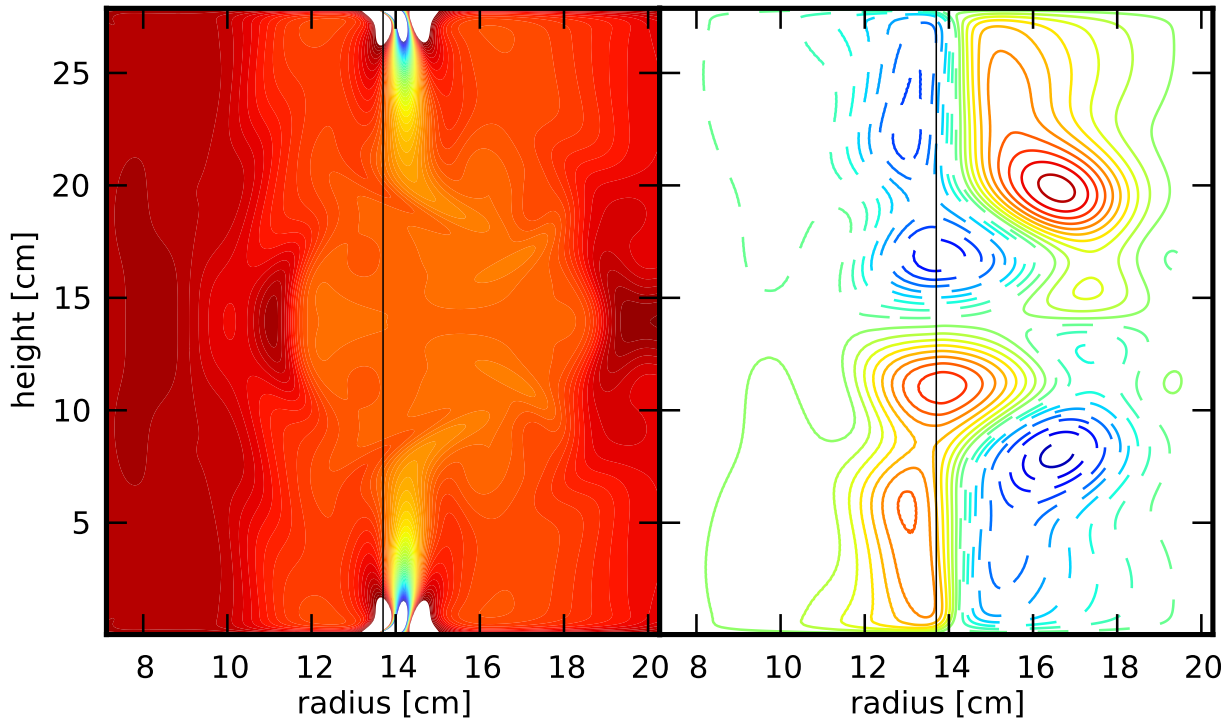

FIG. 6. Snapshot of a numerical simulation of the experiment, for (350, 100), no applied field. *Left:* Shear, $q = (r/\Omega)\,\partial\Omega/\partial r$, versus radius and height. Note the shear layer extending vertically from the ring junction. *Right:* Contours of the poloidal stream function versus radius and height. Contours range from -22 to 22 cm^2/s, in steps of 2. The vertical lines in both figures indicate the location of the inner ring-outer ring junction.

The cause of the emergence of the instability is likely the re-establishment of the globally-unstable shear layer, and the cause of the re-establishment of the shear layer is the Lorentz force due to the applied magnetic field. Again, we can turn to simulations to illustrate this phenomenon. In Figure 9 is presented the same rotation rates as in Figure 7, (400, 100), but now with an applied field of 800 G. This field strength is considered weak since the Elsasser number, $\Lambda = B^2/(\mu_0\rho\eta\Delta\Omega)$, a measure of the ratio of the Lorentz and Coriolis forces, is less than one. In this case the shear layer is only mildly affected by the Lorentz force, with the shear layer still strongly pushed radially outward. We expect that this shear layer, like its hydrodynamic cousin, is merely locally unstable. As the field strength is increased, as in Figures 10-12, the secondary circulation is suppressed, allowing the shear layer to become more and more parallel to the applied field. Again, we would expect that this layer would become unstable to a global hydrodynamic Kelvin-Helmholtz instability, destabilizing the

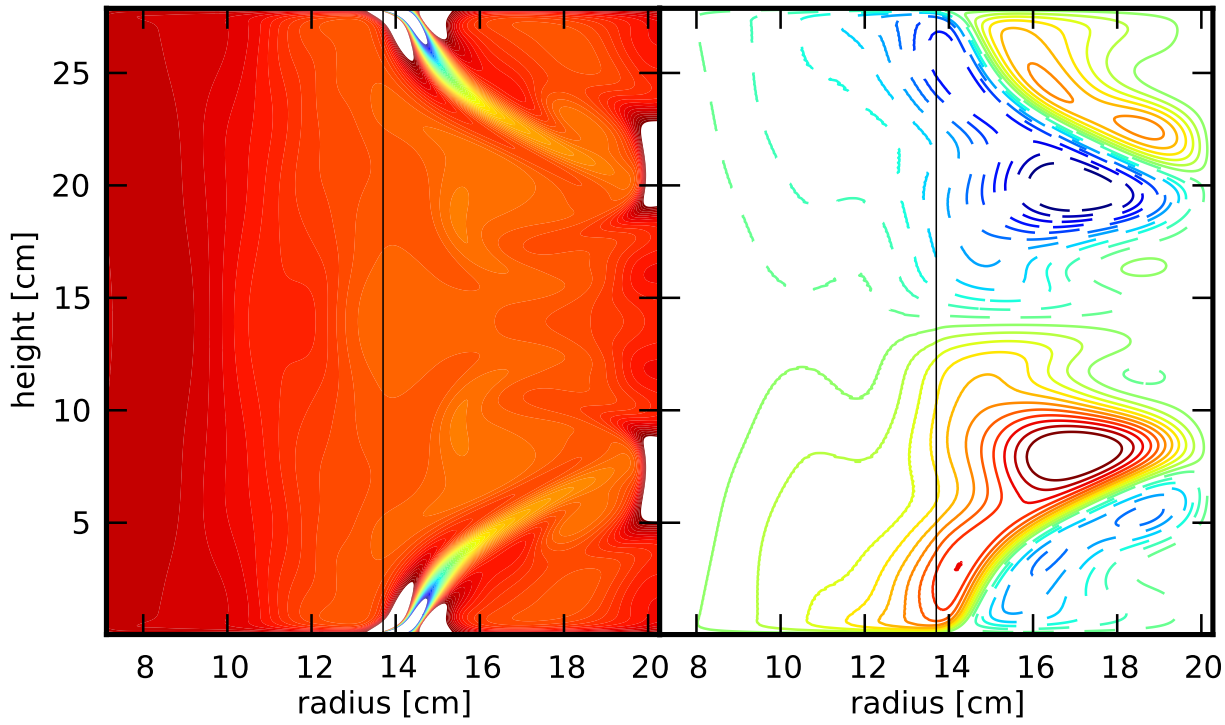

FIG. 7. Numerical simulation of (400, 100), no applied field. The plotting convention is the same as in Figure 6.

bulk flow as observed in the experiment. In these cases the magnetic field plays the role that the Coriolis force plays in the establishment of free shear layers in the hydrodynamic case.

As implied by the simulation results, there is a minimum value of magnetic field required for the shear layer to become globally unstable, roughly corresponding to the field needed to suppress the secondary circulation enough to allow the shear layer to couple to the bulk of the fluid. This transition has been mapped out experimentally, and its instability space is presented in Figure 13, for runs with $Ro = 2.35$. The instability demonstrates the same dependence on Elsasser number as reported previously[22], namely $\Lambda = 1$, though in this case it is the differential speed at the inner ring-outer ring junction which is used in the denominator of the Elsasser number. It should be noted that in the report by Roach *et al.* $\Omega_2 = 0$ for most of the study, and thus $\Delta\Omega = \Omega_1$ and the Elsasser number was defined equivalently as here. Revisiting Figures 9 ($\Lambda = 0.25$) and 10 ($\Lambda = 1.0$) we can see the effect of the magnetic field on the shear layer more directly, again noting that the shear layer curves into the fluid volume when $\Lambda = 1$.

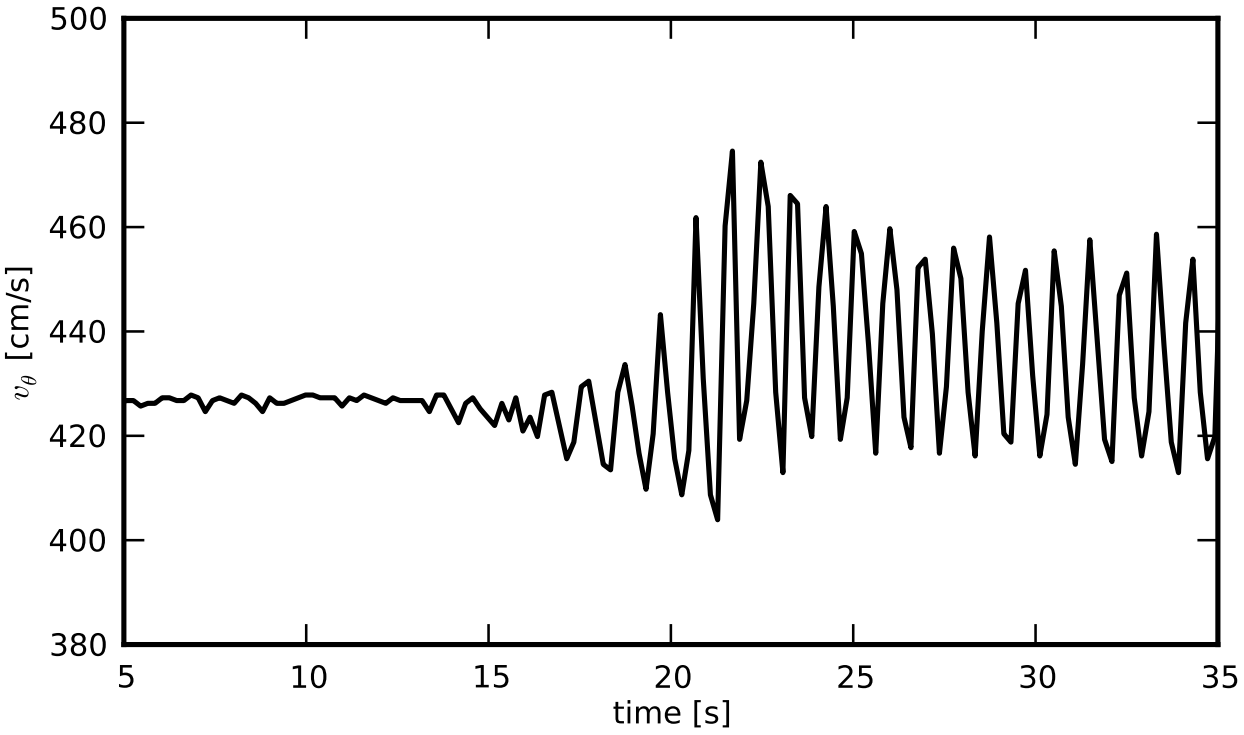

FIG. 8. Azimuthal velocity at $r = 18.2$ cm versus time, measured at the midplane, for (670, 200), 3440 G. The magnetic field turns on at $t = 10$ s.

V. DISCUSSION AND CONCLUSION

A minimum critical Rossby number is required to suppress the global instability of the hydrodynamic free shear layer. In Figure 5 experimental data is presented which suggests that this Rossby number is a constant, $Ro = 2.35$, though admittedly over a range of Ekman number of only one order of magnitude. However the simulations do not confirm this behavior exactly: we hypothesize that the $Ro = 2.5$ case (Figure 6) is globally unstable, due to its erect shear layer, while $Ro = 3.0$ (Figure 7) is only locally unstable, since the shear layer is pushed radially outward. This Rossby number dependence on the orientation of the shear layer has also been produced by simulations at other speeds, with $\Omega_2 = 50$ and $\Omega_2 = 500$. If these simulations are a faithful representation of the experiment then this suggests that the critical Rossby number is not a constant with respect to Ekman number. If this is the case, then the dependence on Ekman number must be extremely weak, with $Ro = 2.35$ when $E \sim 10^{-6}$ in the experiment and $2.5 < Ro < 3.0$ when $E \sim 10^{-4}$ as in the simulations. This very slight change in critical Rossby number might be better explained

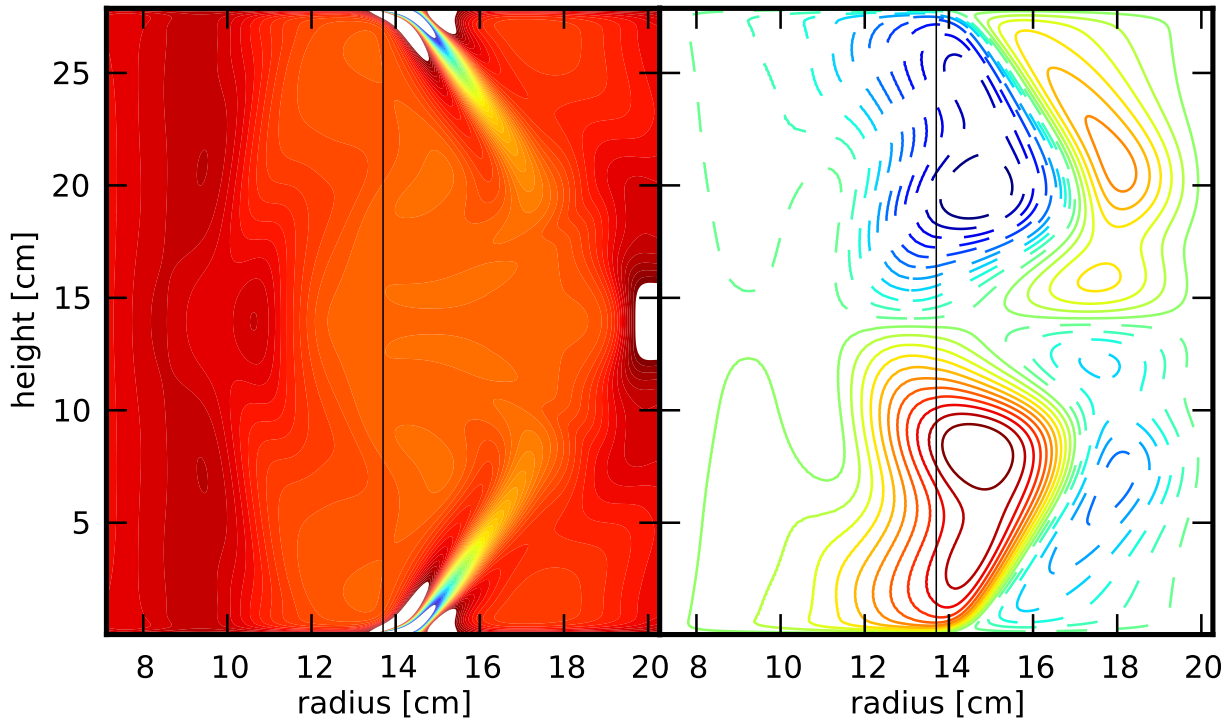

FIG. 9. Numerical simulation of (400, 100), 800 G ($\Lambda = 0.25$). The plotting convention is the same as in Figure 6.

either by imperfections in the simulation's representation of the experiment, perhaps slight differences in geometry, or perhaps is a result of three-dimensional effects which are not captured by the simulation. Experimental and numerical studies of this topic are ongoing.

An outstanding question is that of the value of the critical Rossby number itself: why $Ro = 2.35$? Clearly as the Rossby number is increased significantly above unity the inertial forces due to the secondary circulation become at least as important as the forces due to rotation. As well, the centrifugal force due to the faster rotation rate of the inner parts tends to push the faster flow, and thus the shear layer, into the outer portion of the fluid domain. Clearly these effects are dependent on the fluid being used, in particular the fluid's density, and the geometry of the system involved. This is consistent with a report by Rabaud and Couder[11], who indicate that their apparatus still displays global instability when $Ro > 4.0$ (see their Figure 5), while using a very different working fluid (air) and experimental aspect ratio ($h/r_0 = 0.05 - 0.4$). This is also consistent with results by Edlund, who reports a critical Rossby number of $Ro \sim 2.0$, for an experiment using water in an aspect ratio similar to that of the Princeton MRI experiment. The Rossby number's geometric and fluid

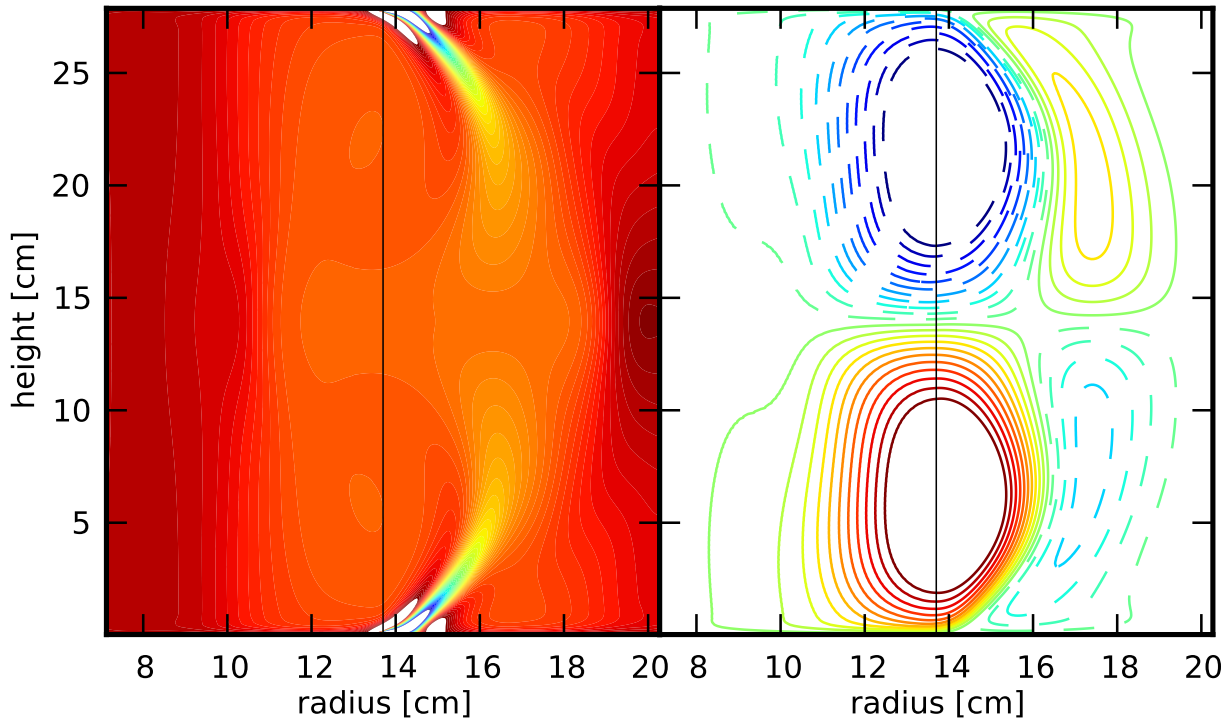

FIG. 10. Numerical simulation of (400, 100), 1600 G ($\Lambda = 1.0$). The plotting convention is the same as in Figure 6.

dependence will be a topic of future study.

One interesting result of this study is the persistent feature of the $\Lambda = 1$ stability criteria for the MHD free-shear layer. One might have expected that the global rotation, which brings with it the stabilizing effect of the Coriolis force, would have caused the stability line to be modified, with less magnetic field needed to re-establish the shear layer, especially since the data in Figure 13 are for the marginally-globally-stable case $Ro = 2.35$. Perhaps the lack of change of criteria is not surprising when one considers the fact that the measurements presented here are at a large Rossby number, in the regime where the secondary flow is as important as rotation. In that case one might expect that the Lorentz force would be more important than Coriolis in suppressing poloidal circulation, and the effects of global rotation would be minimal, as observed. One might also wonder why the Elsasser number is dependent on $\Delta\Omega$ instead of the global rotation rate, Ω_2. The simulations indicate that the magnitude of the current induced in the area of the ring junction is proportional to the shear in that region, and thus proportional to $\Delta\Omega$. Since it is the induced current interacting with the background applied field that generates the Lorentz force, it follows that it is $\Delta\Omega$

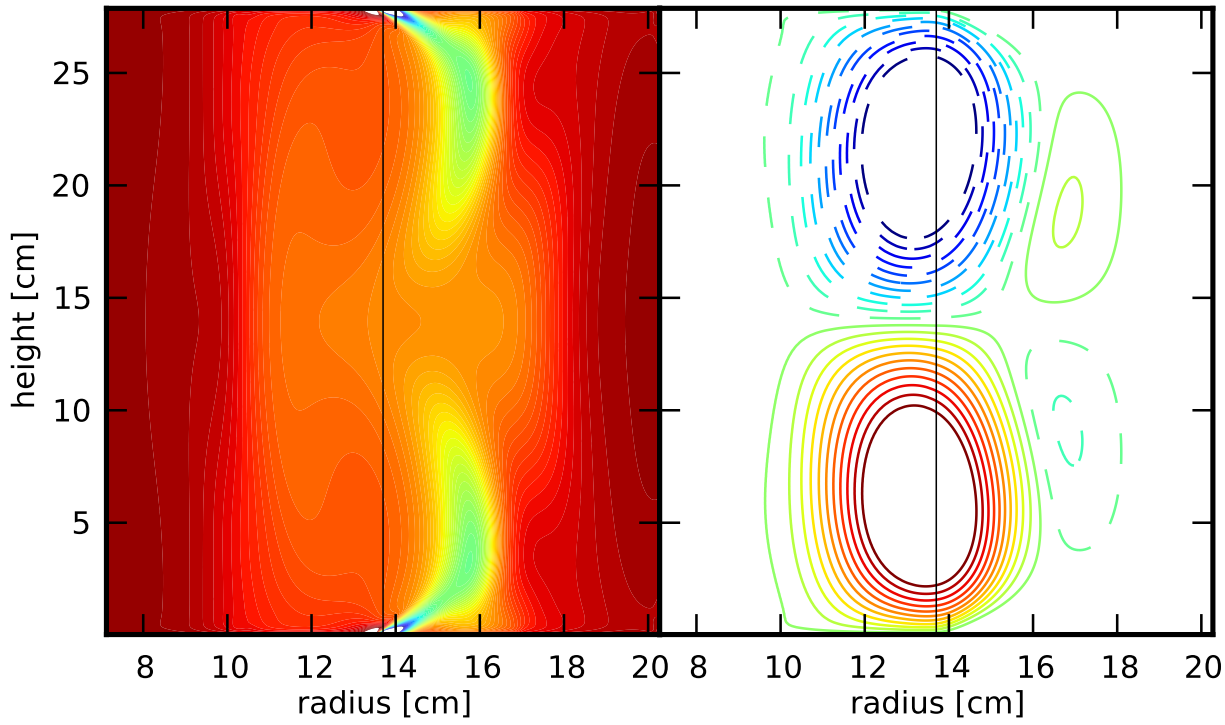

FIG. 11. Numerical simulation of (400, 100), 3580 G ($\Lambda = 5.0$). The plotting convention is the same as in Figure 6.

that is the important speed to consider in the determination of the relative strength of the applied field.

In the simulation results presented in Figure 6, the hydrodynamic shear layer penetrates almost a quarter of the way into the bulk of the fluid. However there is an azimuthally oriented UDV transducer placed 3 centimeters above the lower endcap rings in the experiment, and no such shear layer is observed, though evidence of a hydrodynamic shear layer has been observed when the transducer is tilted such that it can measure about 1 centimeter above the endcap rings. Why are the shear layers in the simulations observed deep in the fluid, while in the hydrodynamic experiments they are not? The most likely explanation lies in the viscosity used in the simulations, which is 300 times larger than in the experiment. Such a large viscosity acts as a stabilizing force on the shear layer, allowing it to penetrate farther into the fluid. Nonetheless, despite its low viscosity, one would expect that the shear layer would be stable farther into the fluid if the experiment could be run at lower Ekman number, increasing the relative strength of the Coriolis force, and Rossby numbers which are below the initial transition to global instability. This effect is observed

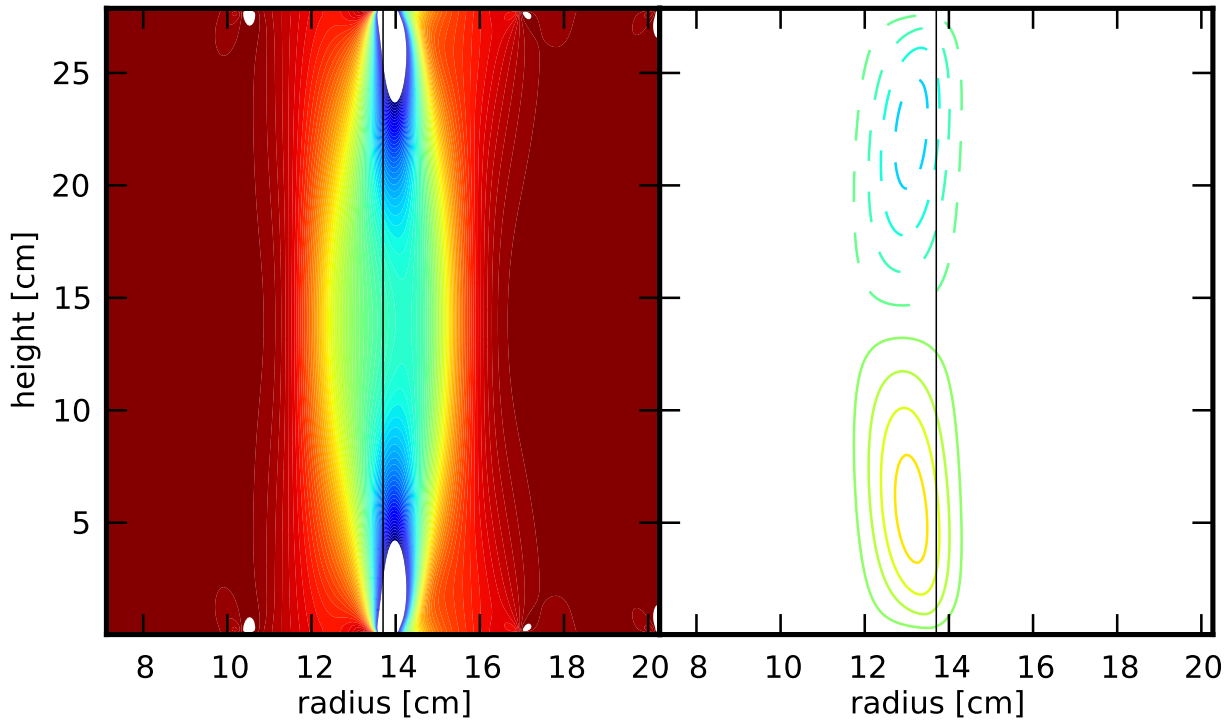

FIG. 12. Numerical simulation of (400, 100), 11310 G ($\Lambda = 50.0$). The plotting convention is the same as in Figure 6.

in the experiment when run with strong relative magnetic fields, meaning at large Elsasser number. In these cases, and as observed in the simulation presented in Figure 12, the shear layer is sufficiently stabilized by the Lorentz force that it can be directly measured at the midplane of the experiment. This has not yet been observed in cases with global rotation, as presented in this work, though it has been measured in cases where the outer ring and outer cylinder are stationary[22].

The 2D numerical simulations presented here indicate that if there is any discontinuity in the velocity field boundary condition a shear layer forms no matter the value of the Rossby or Elsasser numbers. The main question which has been the theme of this paper is: under what conditions does this shear layer generate a globally unstable mode which results in the observations made in the experiment, and under what conditions does it merely decompose into local turbulence? In the case of hydrodynamic shear layers, it seems plausible that the effect of increasing the Rossby number is to cause inertia to push the shear layer into the wall, preventing the layer from, through the Coriolis force, causing the whole fluid volume to become globally unstable. In the case of MHD shear layers, the effect of the applied

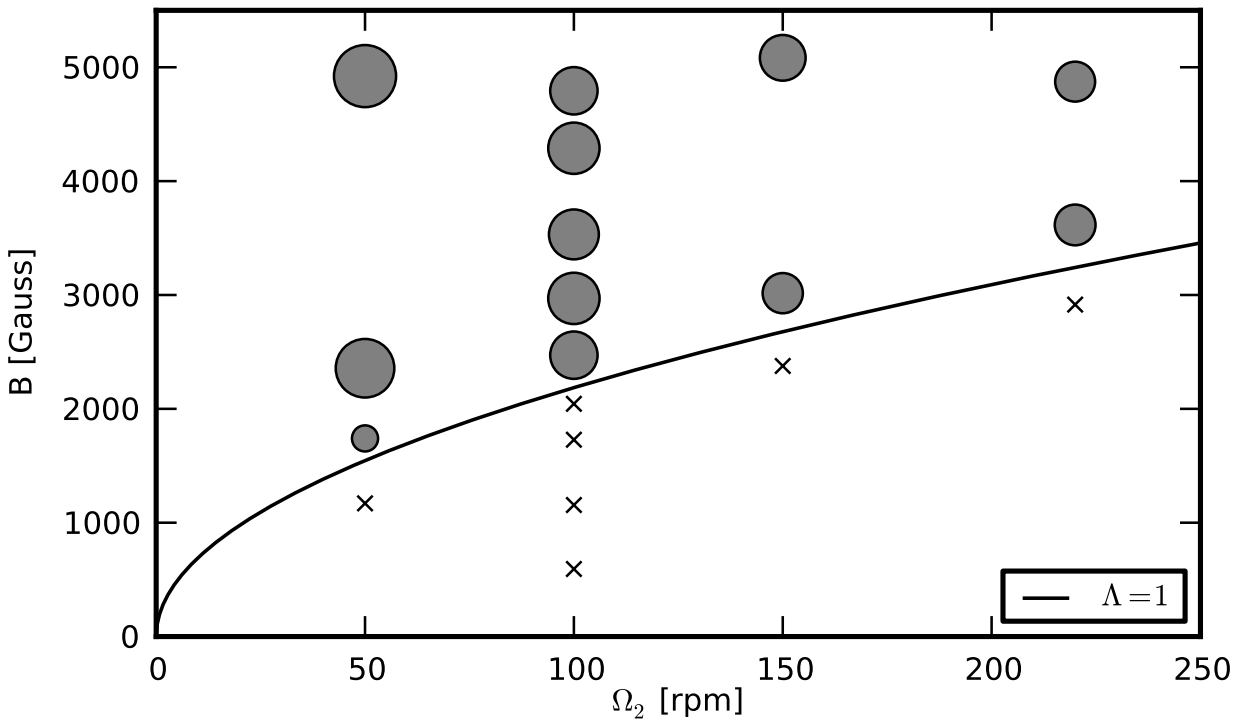

FIG. 13. Experimental shear-layer global-instability space. Dots indicate instability, 'x's indicate stability. The area of the dots is proportional to the power in the oscillations, normalized by $(\Delta\Omega)^2$. All runs were performed with $Ro = 2.35$. The instability space is separated by the $\Lambda = 1$ line, where the Elsasser number is defined here as $\Lambda = B^2/(\mu_0 \rho \eta \Delta\Omega)$.

magnetic field is to suppress the secondary circulation, allowing the globally-stable shear layer to pull away from the wall and, through the Lorentz or Coriolis forces, or both, cause a global instability to ensue. Unfortunately this remains merely a plausible hypothesis, as this cannot be confirmed with the 2D simulations used here. A fully 3D simulation is needed to resolve this issue and is currently being pursued.

In summary, we have presented a study of the role of global rotation on the formation and stability of hydrodynamic and magnetohydrodynamic shear layers. We have demonstrated that there is a critical Rossby number above which hydrodynamic free shear layers are suppressed and cease to be globally unstable, a failure explained by simulations to be one of the shear layer being pushed outward by secondary circulation. Experimental measurements indicate that these suppressed shear layers can be re-established as globally unstable by an applied field. Simulations have shown the cause of the re-establishment of the instability to be the straightening of the shear layer due to the suppression of the poloidal circulation by

the field.

ACKNOWLEDGMENTS

The authors gratefully thank C. Gissinger for useful discussions about these results. This work has been supported by the U.S. Department of Energy's Office of Sciences - Fusion Energy Sciences Program through contract number DE-AC02-09CH11466, the U.S. National Science Foundation under grant numbers AST-0607472 and PHY-0821899, and the U.S. National Aeronautics and Space Administration (NASA) under grant numbers APRA08-0066 and ATP06-35.

REFERENCES

[1]N. Gillet, N. Schaeffer, and D. Jault, Phys. Earth & Planet. Inter. **187**, 380 (2011).

[2]C. A. Jones, Ann. Rev. Fluid Mech. **42**, 583 (2011).

[3]C. Peralta and A. Melatos, Astrophys. J. **701**, L75 (2009).

[4]R. Arlt and G. Rüdiger, Mon. Not. R. Astron. Soc. **412**, 107 (2011).

[5]I. Proudman, J. Fluid Mech. **1**, 505 (1956).

[6]K. Stewartson, J. Fluid Mech. **3**, 17 (1957).

[7]R. Hide and C. W. Titman, J. Fluid Mech. **29**, 39 (1967).

[8]R. Hollerbach, B. Futterer, T. More, and C. Egbers, Theor. Comp. Fluid Dyn. **18**, 197 (2004).

[9]R. Hollerbach, Proc. R. Soc. London, Ser. A **444**, 333 (1994).

[10]E. Dormy, P. Cardin, and D. Jault, Earth Planet. Sci. Lett. **160**, 15 (1998).

[11]M. Rabaud and Y. Couder, J. Fluid Mech. **136**, 291 (1983).

[12]H. Niino and N. Misawa, J. Atmos. Sci. **41**, 1992 (1984).

[13]J. M. Chomaz, M. Rabaud, C. Basdevant, and Y. Couder, J. Fluid Mech. **187**, 115 (1988).

[14]W.-G. Früh and P. L. Read, J. Fluid Mech. **383**, 143 (1999).

[15]F. H. Busse, J. Fluid Mech. **33**, 577 (1968).

[16]R. Hollerbach, J. Fluid Mech. **492**, 289 (2003).

[17]N. Schaeffer and P. Cardin, Nonlin. Proc. Geophys. **12**, 947 (2005).

[18]N. Schaeffer and P. Cardin, Phys. Fluids **17**, 104111 (2005).

[19]X. Wei and R. Hollerbach, Phys. Rev. E **78**, 026309 (2008).

[20]B. Lehnert, Proc. R. Soc. London, Ser. A **233**, 299 (1955).

[21]D. R. Sisan, N. Mujica, W. A. Tillotson, Y.-M. Huang, W. Dorland, A. B. Hassam, T. M. Antonsen, and D. P. Lathrop, Phys. Rev. Lett. **93**, 114502 (2004).

[22]A. H. Roach, E. J. Spence, E. E. Edlund, P. Sloboda, and H. Ji, "Observation of a free-Shercliff-layer instability in cylindrical geometry", in press, *Phys. Rev. Lett.*

[23]X. Wei and R. Hollerbach, Ann. Math. **215**, 1 (2010).

[24]C. Gissinger, H. Ji, and J. Goodman, Phys. Rev. E p. 026308 (2011).

[25]C. Gissinger, J. Goodman, and H. Ji, "The role of boundaries in the MagnetoRotational Instability", submitted to *Phys. Fluids*.

[26]E. Schartman, H. Ji, and M. J. Burin, Rev. Sci. Inst. **80**, 024501 (2009).

[27]D. Brito, H.-C. Nataf, P. Cardin, J. Aubert, and J. Masson, Experiments in Fluids **31**, 653 (2001).

[28]J. C. Hayes, M. L. Norman, R. A. Fiedler, J. O. Bordner, P. S. Li, S. E. Clark, A. ud Doula, and M.-M. M. Low, Astrophys. J. Suppl. **165**, 188 (2006).

[29]W. Liu, J. Goodman, and H. Ji, Astrophys. J. **643**, 306 (2006).

[30]W. Liu, J. Goodman, I. Herron, and H. Ji, Phys. Rev. E **74**, 056302 (2006).

[31]W. Liu, Astrophys. J. **684**, 515 (2008).

[32]D. J. Baker, J. Fluid Mech. **29**, 165 (1967).

[33]W. L. Siegmann, J. Fluid Mech. **64**, 289 (1974).

The Princeton Plasma Physics Laboratory is operated
by Princeton University under contract
with the U.S. Department of Energy.

Information Services
Princeton Plasma Physics Laboratory
P.O. Box 451
Princeton, NJ 08543

Phone: 609-243-2245
Fax: 609-243-2751
e-mail: pppl_info@pppl.gov
Internet Address: http://www.pppl.gov